OPEN ACCESS Freely available online

AFM Applied Functional Materials

ISSN 2737-5323
Volume 2, Issue 1
https://www.iikii.com.sg/journal/AFM
Applied Functional Materials

Influence of $MAPBI_3$ Annealing Temperature on Perovskite Solar Cell

Tung-Lung Wu [1], Jenn-Kai Tsai [2, *], Ya-Zhu Song [2], Tang-Kai Chen [2], Tian-Chiuan Wu [2], Kao-Wei Min [3], Ming-Ta Yu [4] and Chi-Ting Ho [4]

[1] School of Mechanical and Automotive Engineering, Zhaoqing University, Zhaoqing, Guangdong 516260, China
[2] Department of Electronic Engineering, National Formosa University, Yunlin County 632, Taiwan
[3] College of Engineering, National Formosa University, Yunlin County 632, Taiwan
[4] Department of Mechanical Design Engineering, College of Engineering, National Formosa University, Yunlin County 632, Taiwan
* Correspondence: tsaijk@nfu.edu.tw

Received: Feb 1, 2022; **Accepted:** Mar 1, 2022; **Published:** Mar 30, 2022

Abstract: This study mainly is carried out to discuss the effect of nitrogen annealing temperature on perovskite solar cells. The annealing temperature affects perovskite solar cells during the annealing process. It also affects the formation of perovskite crystals. Perovskite crystals need to form in a nitrogen box for manufacturing Perovskite solar cells. Spin-coating $MAPbI_3$ on the substrate is annealed with a nitrogen furnace tube to form perovskite crystals. The remaining PbI_2 after the annealing is completed to improve the efficiency of perovskite solar cells. The optimal temperature for the formation of perovskite crystals is found by adjusting the annealing temperature. By using UV-visible spectrometer, field emission-scanning electron microscope, and measurements of photoelectric conversion efficiency, cell structure and optoelectronic properties are analyzed as the final results.

Keywords: Perovskite, $MAPBI_3$, Annealing temperature, Solar cell

1. Introduction

Organic-inorganic lead halide perovskites have emerged as an effective photovoltaic element with unique properties for photovoltaic applications, including high absorption coefficients, tunable bandgaps, and solution handling capabilities [1,2]. The improvement of the photoelectric conversion efficiency (PCE) of perovskite solar cells (PSCs) is dependent on how to control the shape, interface defects, and passivation of perovskite thin films [3]. Therefore, it is important to choose an effective deposition technique. One-step spin-coating, two-step spin-coating, sequential deposition, and vapor deposition have been widely used to fabricate high-quality perovskite thin films [4]. Although two-step spin-coating and sequential deposition are complex, they show good repeatability and high controllability. Vapor deposition is appropriate for the film uniformity of high-density planar components. The crystallization deposition in traditional one-step spin-coating is difficult to control. In addition, the humidity and temperature of the coating seriously affect it. The thermal annealing process involves the evaporation of organic solvents and volatile components. Different annealing temperatures change the growth of perovskite crystals on the surface, thereby affecting the efficiency of perovskite solar cells [5–8].

In this study, we use lead iodide (PbI_2) and methylamine iodide (MAI) mixed with dimethylformamide (DMF) and dimethyl sulfoxide (DMSO) as perovskite solutions in the fabrication of $MAPbI_3$ perovskite layers. Since DMF and DMSO require different annealing temperatures [11–13], we experiment with different annealing temperatures to understand the effect on perovskite solar cells and to find the optimal temperature for the formation of perovskite crystals [10].

2. Experimental methods

The fabrication of perovskite solar cells is shown in Figure 1. Firstly, we use ultrasonic washing to clean the conductive glass in acetone, methanol, and deionized water for 15 min, respectively. Secondly, we put the cleaned FTO glass into the drying oven for 30 min, and then put it in the ultraviolet disinfection cabinet for 10 min. Thirdly, we prepare the dense TiO_2 layer [14] and spin-coat the solution of dense TiO_2 on clean FTO glass at 5000 RPM for 30 s. After that, the glass is annealed in a high-temperature furnace at 500 °C for 30 min. Fourthly, the mesoporous TiO_2 layer is prepared and spin-coated with TiO_2 solution at 3000 RPM for 30 s. Then, the finished mesoporous TiO_2 layer was placed in a high-temperature furnace for annealing at 500 °C for 60 min. Next, the perovskite precurse solution including MAI and PbI_2 (1:1.2 mol/L) are dissolved in a mixed solution of N,N-dimethylformamide (DMF, 400 μL) and dimethyl sulfoxide (DMSO, 100 μL). Then, the solution is heated at 70°C and stirred for 1.5 h until it is completely dissolved [16]. The $MAPbI_3$ solution is spin-coated on the $MAPbI_3$ and the compact TiO_2/mesoporous TiO_2 layer at

2000 and 5000 RPM for 20 and 30 s. During the spin-coating process, chlorobenzene is added dropwise to promote the crystallization of the perovskite. Finally, the crystal is annealed at 110°C for 20 min.

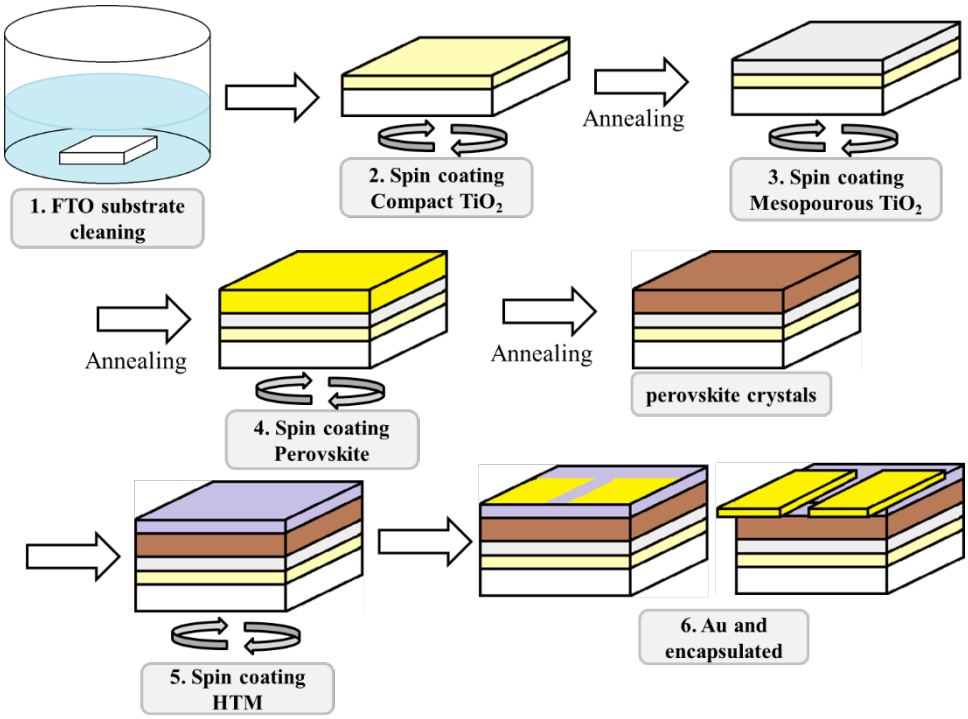

Fig. 1. Illustration of the fabrication process of the PSCs.

The prepared electrokinetic transport layer solution was spin-coated at a speed of 4000 RPM for 30 s to prepare a hole transport layer on the perovskite film. Finally, gold is plated on the hole transport layer, and gold electrodes are prepared to complete the perovskite solar cell.

3. Results

3.1. Perovskite

We use the one-step spin-coating method to fabricate the perovskite layer. Before making it, we fill the homemade glove box with nitrogen until the relative humidity inside the glove box falls below 15% to spin-coat. An anti-solvent is added during the spin coating process, allowing the perovskite solution to grow into perovskite crystals smoothly. The $MAPbI_3$ organometallic mixed solution prepared by MAI and PbI_2 is used with a molar concentration ratio of 1:1.2. After fixing the concentration of MAI and PbI_2 [9], we anneal it at different temperatures of 90, 100, 110, and 120°C. Since organic solutions are sensitive to temperature changes, DMF is generally used in the preparation of perovskite layers. In this study, DMSO is added to DMF so that the perovskite crystals grow uniformly. However, suitable annealing temperatures for DMF and DMSO are different. The annealing temperature of DMSO is generally higher than that of DMF. Therefore, according to the perovskite cells made of DMF, the most commonly used annealing temperature is 100°C as a reference, and three additional temperatures are set. The effect of different temperatures on the growth of crystalline perovskite-organometallic mixed solutions was observed. The experimental results are measured and analyzed by UV-visible spectrometer (UV-vis), field emission-scanning electron microscope (SE-SEM), X-ray diffractometer (XRD), incident photon-to-electron conversion efficiency (IPCE), and photoelectric conversion efficiency.

3.1.1. SEM analysis

A scanning electron microscope is mainly used to observe the surface of materials, whose resolution reaches the nanometer level. The electron gun generates a high-energy electron beam through the principle of thermal ionization or field emission. After passing through the electromagnetic lens group, the electron beam is focused on the test piece. The electron beam is deflected by the scanning coil in the middle for a second-dimensional scan on the test piece. Generally, the SEM structure photo of the material is formed by using the secondary electrons and backscattered electrons generated when the electron beam is in contact with the test piece. Then, the secondary signal is processed to form an observable SEM structure photo. Figure 2 shows that the surface phase of

perovskite is similar at other temperatures except for 90°C, and perovskite crystal is formed by annealing at 110°C. The film thickness is about 375–430nm, which is the most appropriate thickness at all temperatures.

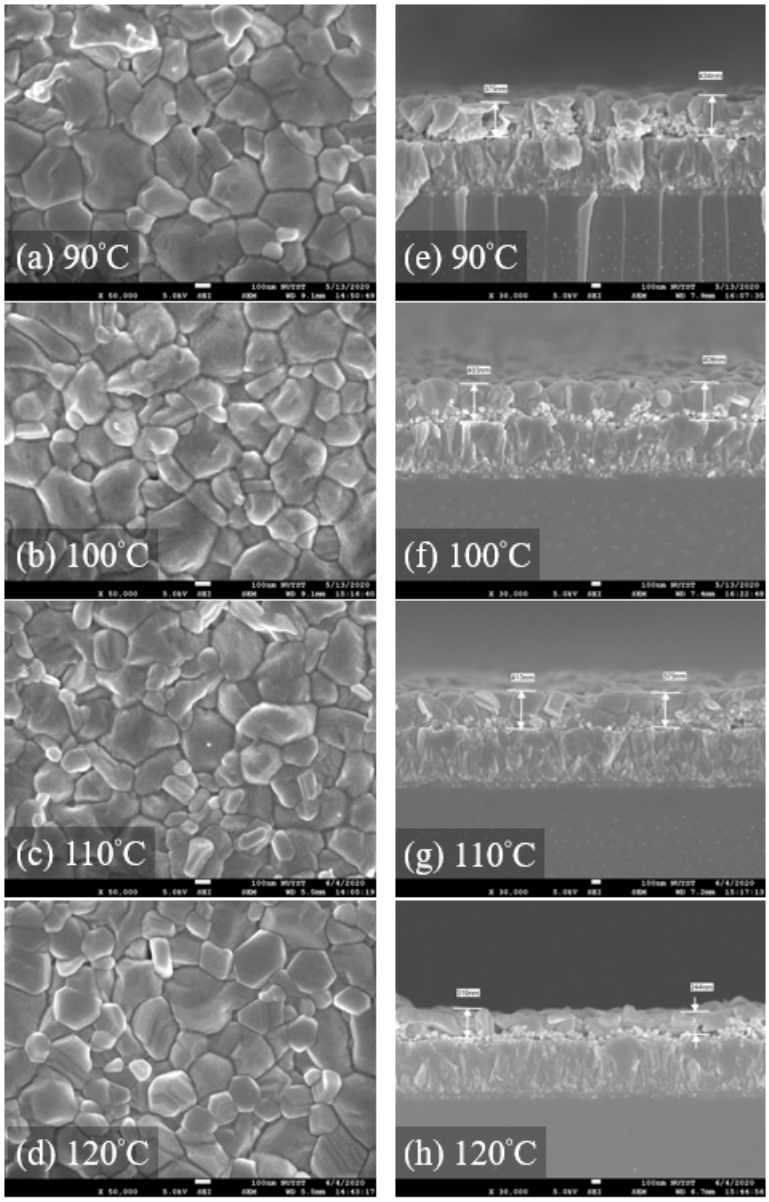

Fig. 2. SEM images of samples, perovskite/ compact TiO_2/ mesoporous TiO_2/FTO layers, annealed at different temperatures.

Table 1. Perovskite thickness of perovskite layer annealed at different temperatures

	90°C	100°C	110°C	120°C
Thickness (nm)	375~400	400~420	375~430	250~320

3.1.2. XRD analysis

Generally, the wavelength of an X-ray is similar to the distance between atoms in a solid. Therefore, a crystalline crystal is grating for X-ray. When an X-ray is irradiated on the crystal, diffraction occurs. The diffraction intensity of X-rays is calculated using Bragg's law ($n\lambda = 2d_{hkl} \sin\theta$, λ is the wavelength of the X-ray, d is the spacing, θ is the diffraction angle, n is a positive integer, and hkl is the index of each crystal plane). The XRD spectrum is composed of the position (2θ) and the intensity (I) of the diffraction peak. The position (2θ) of the diffraction peak shows the shape and size of each lattice on the crystal. The intensity of the diffraction peak shows the atomic species and positions of the internal composition of the crystal. Therefore, we perform XRD analysis for samples annealed at different annealing temperatures structure. Figure 3 shows the XRD analysis results using a wavelength of 1.5406 Å X-ray.

According to the analysis, 14.22° (110), 28.66° (220), and 32.01° (310) are the lattice peaks of $MAPbI_3$. In Figure 3, "●" is the lattice peak of $MAPbI_3$ and "◇" is the lattice peak of TiO_2/FTO, a larger peak is found after annealing at annealing temperature of 110°.

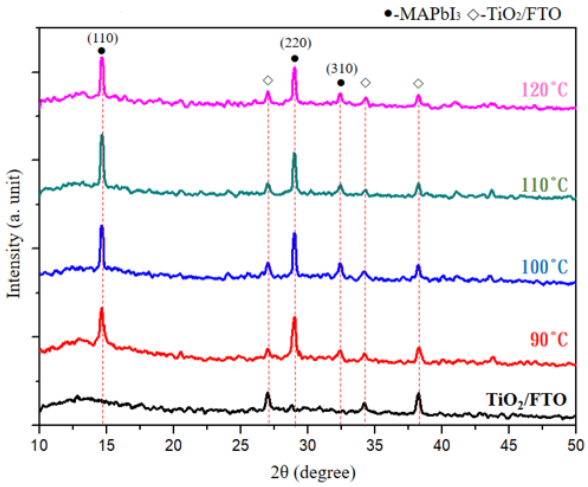

Fig. 3. XRD analysis chart of samples after different temperatures annealed.

3.1.3. UV-Vis analysis

UV-visible spectrometers use different light energies to excite electrons to generate different electron transitions, whose range is between ultraviolet (UV) and visible light (VIS). When the light of different wavelengths irradiates the sample continuously, the absorption intensity corresponding to the wavelength is obtained. Figure 4 shows the UV-Vis absorption spectra of samples at different annealing temperatures. The highest peak is the longest wavelength about 500 nm at sample after 110°C annealing, which means that the perovskite film has better solar light absorption at 110°C annealing temperature.

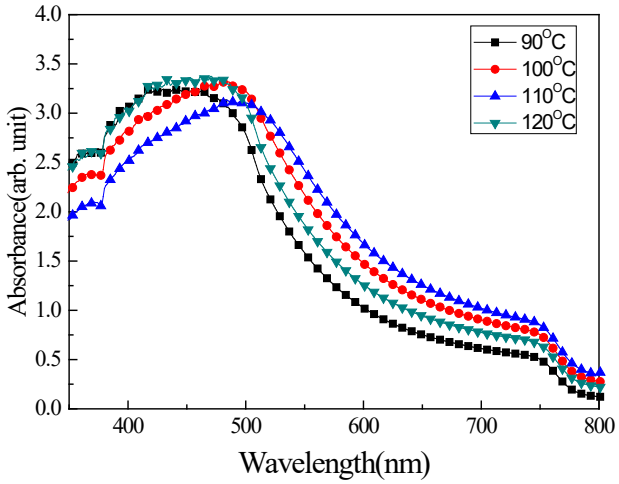

Fig. 4. UV-Vis absorption of samples after different temperatures annealed.

3.2. Analysis of perovskite solar cells

3.2.1. IPCE

$$SR\left(\frac{A}{W}\right) = \frac{I_{SC}}{P_{IN}} \quad (1)$$

$$IPCE(\%) = \frac{1240 \times SR}{\lambda} \times 100\% \quad (2)$$

Equation (1) is for the spectral response (SR). P_{IN} is the energy of the incident light, and I_{SC} is the current converted by the solar cell after receiving the incident light, also known as the short-circuit current. Equation (2) is for IPCE, where λ is the incident wavelength. The spectral response displays the photoelectric conversion efficiency of the solar cell for different wavelengths. By using the spectral response or IPCE spectrogram, we analyze the quality of the solar cell as reference data for improvement.

Figure 5 shows the result of the IPCE analysis of the perovskite solar cell fabricated by annealing at temperature of 110°C. The conversion efficiency gradually decrease at wavelength longer than 500 nm and steep drop at 740 nm have been observed.

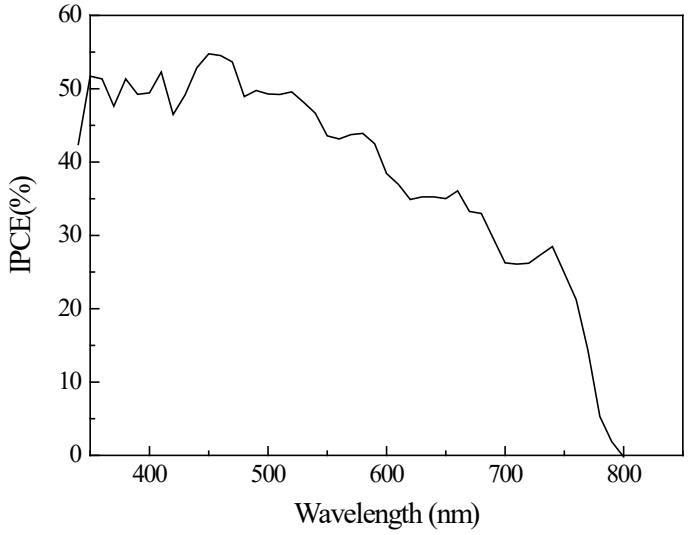

Fig. 5. IPCE spectrum of perovskite solar cell.

3.2.1. Power Conversion Efficiency

Power conversion efficiency (PCE) is defined as the ratio of energy output from the solar cell to input light energy from the sun, it calculated by dividing maximum power (P_{MAX}) by solar energy (E) (see in Equation (3)). The standard value of solar energy (E) is 100 mW/cm^2. In addition, PCE is calculated by dividing $V_{OC} \times J_{SC} \times$ F.F. by P_{IN} (Eq. (4)). P_{IN} is the power density of the incident light source.

$$PCE = \frac{P_{MAX}}{E} \quad (3)$$

$$PCE = \frac{J_{SC} \times V_{OC} \times F.F.}{P_{IN}} \quad (4)$$

Fill factor (F.F.) is a reference value defined by PCE. If the maximum power point of the solar cell falls on the vertical intersection of the open-circuit voltage (V_{OC}) and the short circuit current density (J_{SC}) ideally, the maximum power can be obtained.

However, due to the physical limitations of the battery structure, process technology, and materials, the battery cannot achieve the ideal output power. Therefore, the fill factor (F.F.) is defined as follows.

$$F.F. = \frac{I_{MAX} \times V_{MAX}}{J_{SC} \times V_{OC}} \times 100\% \quad (5)$$

When $I_{MAX} = J_{SC}$, $V_{MAX} = V_{OC}$, and FF = 100%, the quality of the solar cell is judged or referred to as comparison with the value of F.F..

Figure 6 shows perovskite solar cells tested at different annealing temperatures. Figure 6 and Table 2 present that as the annealing temperature increases, the open-circuit voltage and short circuit current density increase. The photoelectric conversion efficiency becomes the best at 110°C, but the efficiency decreases at 120°C. According to the experimental results, maybe because of insufficient temperature, perovskite solar cells annealing at 90 and 100 °C do not reach the optimal crystalline state. According to Fig. 2, due to high temperature, the part of the organic solution of perovskite solar cells volatilizes when the perovskite crystal is annealed, resulting in a decrease in the efficiency of perovskite solar cells at 120°C.

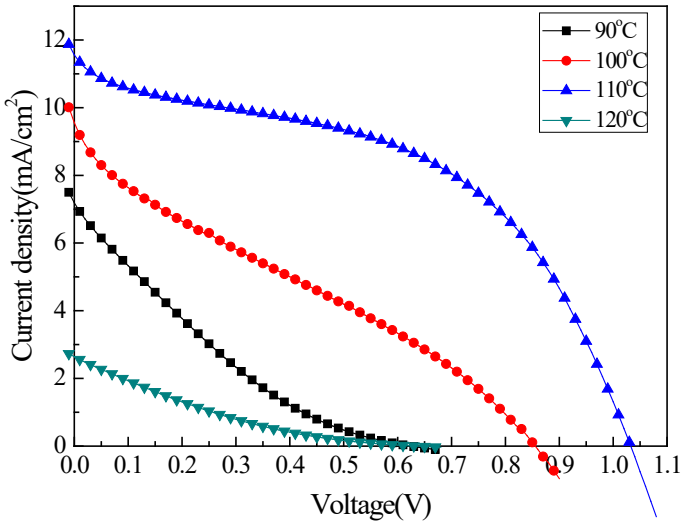

Fig. 6. I-V curves of perovskite solar cells used at different annealing temperatures.

Table 2. I-V characteristic parameters of perovskite solar cells for different annealing temperatures

	V_{OC} (V)	J_{SC} (mA/cm^2)	F.F. (%)	PCE (%)
90°C	0.62	7.18	16.86	0.76
100°C	0.86	9.55	25.59	2.11
110°C	1.03	11.55	46.8	5.63
120°C	0.63	2.64	15.64	0.26

4. Conclusions

The purpose of this study is to understand the changes and the effect of perovskite crystallization on perovskite solar cells by adjusting the annealing temperature. We make the molar concentration MAI and PbI_2 into a 1:1.2, and then anneal the solar cell with nitrogen at four temperatures which are 90, 100, 110, and 120°C to fabricate perovskite solar cells. The results of SEM, XRD analysis, and efficiency measurement reveals that the annealing temperature affects perovskite crystallization as the thickness of perovskite annealed at 110°C is thicker than that at any other temperatures. According to the J-V curve, the photoelectric conversion efficiency becomes the best when the annealing temperature is 110°C. As the annealing temperature decreases, the photoelectric conversion efficiency decreases, too. Finally, the IPCE spectrum, J-V curve, and photoelectric conversion efficiency show that the perovskite solar cells that are annealed at 110 °C become the best cells when compared with other cells made with different methods.

Author Contributions: JKT designed the work and wrote the manuscript. YZS and TKC carried out the preparation of samples, UV–vis absorption, and J-V measurements. TLW, KWM, MTY carried out the measurements and analyses of XRD and IPCE. TCW and CTH helped in carrying out the FESEM measurements. All authors read and approved the final manuscript.

Funding: This research did not receive external funding.

Acknowledgments: The authors would like to thank Meng-Xiu Chen, Yu-Chi Tsao, Teen Hang Meen, and Yu Pin Luo for their assistance. This work was partially supported by the National Science Council of Taiwan, the Republic of China

Conflicts of Interest: The authors declare no conflict of interest.

References

1. Luo, J.; Wang, Y.-X.; Zhang, Q. Progress in perovskite solar cells based on ZnO nanostructures, *Sol. Energy* **2018**, *163*, 289–306.
2. Bretschneider, S.A; Weickert, J.; Dorman, J.A. Schmidt-Mende, Research Update:physical and electrical characteristics of lead halide perovskites for solar cell applications, *Apl. Mater*. **2014**, *2* (4), 6050.
3. Wu, X.; Trinh, M.T.; Niesner, D., Zhu, H.; Norman, Z.; Owen, J.S.; Yaffe, O.; Kudisch, B.J.; Zhu, X.-Y. Trap States in Lead Iodide Perovskites. *J. Am. Chem. Soc.*, **2015**, *137*, 2089.
4. Zhang, Y.; Liu, W.; Tan, F.; Gu, Y. The essential role of the poly (3-hexylthiophene) hole transport layer in perovskite solar cells. *J. Power Sources*, **2015**, *274*, 1224–1230.
5. Eperon, G.E.; Burlakov, V.M.; Docampo, D.; Goriely, A. and Snaith, H.J. Morphological Control for High Performance, Solution- Processed Planar Heterojunction Perovskite Solar Cells. *Adv. Funct. Mater*., **2014**, *24*, 151–157.
6. Dualeh, A.; Tetreault, N.; Moehl, T. ; Gao, P.; Nazeeruddin, M.K.; Gratzel, M. Effect of Annealing Temperature on Film Morphology of Organic–Inorganic Hybrid Pervoskite Solid-State Solar Cells. *Adv. Funct. Mater*., **2014**, *24*, 3250.
7. Xiao, Z.; Bi, C.; Shao, Y.; Dong, Q.; Wang, Q.; Yuan, Y.; Wang, C.; Gao, Y. and Huang, J. Efficient, high yield perovskite photovoltaic devices grown by interdiffusion of solution-processed precursor stacking layers. *Energy Environ. Sci*, **2014**, *7*, 2619–2623.
8. Wang, Q.; Shao, Y.; Xie, H.; Lyu, L.; Liu, X.; Gao, Y.; Huang, J. Qualifying composition dependent p and n self-doping in $CH_3NH_3PbI_3$ *Appl.Phys. Lett*., **2014**, *105*, 163508.
9. Cao, D.H.; Stoumpos, C.C.; Malliakas, C.D.; Katz, M.J.; Farha, O.K.; Hupp, J.T.; Kanatzidis, M.G., Remnant PbI_2, an unforeseen necessity in high-efficiency hybrid perovskite-based solar cells? *APL Materials 2*, **2014**, *2*(9), 091101.
10. van Franeker, J.J.; Hendriks, K.H.; Bruijnaers, B.J.; M. Verhoeven,M.M. Wienk, R.A.J. Janssen, Monitoring thermalannealing of perovskite solar cells with in situ photoluminescence. *Adv. Energy Mater*. 7, 1601822.
11. Soe, C.M.M.; Nie, W.; Stoumpos, C.C; Tsai, H.; Blanconet, J.-C. et.al., Understanding film formation morphology and orientation in high member 2D Ruddlesden–Popper perovskites for high-efficiency solar cells. *Adv. Energy Mater*. **2018**, *8*,1700979.
12. Chen, Y.; Sun, Y.; Peng, J.; Zhang, W.; Su,X. et al..Tailoring organic cation of 2D air-stable organometal halide perovskites for highly efficient planar solar cells. *Adv.Energy Mater*. **2017**, *7*, 1700162.
13. Nie, W.Y.; Tsai, H.H.; Asadpour, R.; Blancon, J.C.; Neukirch, A.J. et al., High-efficiency solution-processed perovskite solar cells with millimeter-scale grains. *Science* **2015**, *347*, 522–525 (2015).
14. Ueoka, N.; Oku, T. "Stability Characterization of PbI_2-Added $CH_3NH_3PbI_3$−xClx," ACS *Appl. Mater. Interfaces*, **2018**, *10* (51), 44443–44451.
15. Ko, H.-S.; Lee, J-.W.; Park, N-G. "15.76% Efficiency Perovskite Solar Cell Prepared under," *Journal of Materials Chemistry A*, **2015,** *3*, 8808–8815.
16. Xiao, M.; Huang, F.; Huang, W.; Dkhissi, Y.; Zhu, Y.; Etheridge, J.; Gray-Weale, A.; Bach, U.; Cheng, Y.B.; Spiccia, L. A fast deposition-crystallization procedure for highly efficient lead iodide perovskite thin-film solar cells, *Angew. Chem*. **2015**, *53* (37) 9898–9903.

Publisher's Note: IIKII stays neutral with regard to jurisdictional claims in published maps and institutional affiliations.

Copyright: © 2022 The Author(s). Published with license by IIKII, Singapore. This is an Open Access article distributed under the terms of the Creative Commons Attribution License (CC BY), which permits unrestricted use, distribution, and reproduction in any medium, provided the original author and source are credited.